

Surface thermophysical properties investigation of the potentially hazardous asteroid (99942) Apophis

LiangLiang Yu¹, Jianghui Ji² and Wing-Huen Ip^{1,3}

¹ Space Science Institute, Macau University of Science and Technology, Taipa, Macau;
yullmoon@live.com

² CAS Key Laboratory of Planetary Sciences, Purple Mountain Observatory, Chinese Academy of Sciences, Nanjing 210008, China; *jijh@pmo.ac.cn*

³ Institute of Astronomy, National Central University, Jhongli, Taoyuan City 32001, Taiwan;
wingip@astro.ncu.edu.tw

Abstract In this work, we investigate the surface thermophysical properties (thermal emissivity, thermal inertia, roughness fraction and geometric albedo) of asteroid (99942) Apophis, using the currently available thermal infrared observations of CanariCam on Gran Telescopio CANARIAS and far-infrared data by PACS of Herschel, on the basis of the Advanced thermophysical model. We show that the thermal emissivity of Apophis should be wavelength dependent from 8.70 μm to 160 μm , and the maximum emissivity may arise around 20 μm similar to that of Vesta. Moreover, we further derive the thermal inertia, roughness fraction, geometric albedo and effective diameter of Apophis within a possible 1σ scale of $\Gamma = 100_{-52}^{+100} \text{ Jm}^{-2}\text{s}^{-0.5}\text{K}^{-1}$, $f_r = 0.78 \sim 1.0$, $p_v = 0.286_{-0.026}^{+0.030}$, $D_{\text{eff}} = 378_{-25}^{+19} \text{ m}$, and 3σ scale of $\Gamma = 100_{-100}^{+240} \text{ Jm}^{-2}\text{s}^{-0.5}\text{K}^{-1}$, $f_r = 0.2 \sim 1.0$, $p_v = 0.286_{-0.029}^{+0.039}$, $D_{\text{eff}} = 378_{-29}^{+27} \text{ m}$. The derived low thermal inertia but high roughness fraction may imply that Apophis could have regolith on its surface, and less regolith migration process has happened in comparison with asteroid Itokawa. Our results show that small-size asteroids could also have fine regolith on the surface, and further infer that Apophis may be delivered from the Main Belt by Yarkovsky effect.

Key words: techniques: thermal infrared — variables: thermal inertia — asteroid: individual: (99942) Apophis

1 INTRODUCTION

(99942) Apophis (2004 MN4) is categorized as an Aten-group near-Earth asteroid (NEA) based on its orbital characteristics. The asteroid was known as a potentially hazardous object (PHO) with a significant

JPL-Sentry and ESA-NEODyS. On December 27, 2004, the Spacewatch survey announced pre-discovery observations (Gilmore et al., 2004) from March 2004, and removed any impact possibility in 2029.

Radar observations of Apophis were obtained by the Arecibo observatory in January 2005, August 2005 and May 2006. More recently, Thuillot et al. (2015) reported new astrometric observations obtained by space-based *Gaia-FUN-SSO* during the Apophis' latest period of visibility from December 21, 2012 to February 5, 2013, and soon afterwards, Wang et al. (2015) published precise 298 CCD position data observed by the ground-based 2.4-m telescope at Yunnan Observatory from February 4, 2013 to March 2, 2013. These observations significantly reduced Apophis' orbital uncertainty and led to a more accurate estimation of the encountering distance about 5-6 Earth radius from the geocenter in 2029 (Gilmore et al., 2008; Thuillot et al., 2015; Wang et al., 2015). Although the 2029 impact has been eliminated, other potential impacts may still exist in the following decades.

Chesley (2005) showed that the Yarkovsky effect (Bottke et al., 2006) significantly affects post-2029 predictions of Apophis' orbit evolution and thus should be taken into account for its impact predictions. As well known, the Yarkovsky effect due to the recoil of reflected and thermal emitted photons is one most important of those non-gravitational effects. Utilizing selected best astrometric and radar data covering the interval from March 15, 2004 to December 29, 2012, Farnocchia et al. (2013) carried out a detail orbital analysis and quantified that predictions of the Earth impacts of Apophis between 2060 and 2105 are sensitive to its physical parameters, including diameter, albedo, rotation period, obliquity, density, and thermal inertia, which determine the rate of Yarkovsky drift of Apophis' semimajor axis. In addition, Vokrouhlický et al. (2015) provided a more advanced estimation of Apophis' Yarkovsky effect, and predicted that Apophis' secular change in the semimajor axis may be $(-12.8 \pm 3.6) \times 10^{-4}$ AU/Myr. Therefore accurate thermal properties (thermal inertia, roughness fraction and so on) and shape model are necessary to predict its Earth impact probability in the following decades in consideration of the significantly important Yarkovsky effect.

By comparing spectral and mineralogical characteristics of likely meteorite analogs from 0.55 to 2.45 μm reflectance spectral measurements of Apophis observed by NASA IRTF and Baade Telescope at the Magellan Observatory, Binzel et al. (2009) found that Apophis appears well classified as an Sq-type and most closely resembles LL ordinary chondrite meteorites, which is rather similar to asteroid Itokawa (Abe et al., 2006).

With the photometric observations of Apophis from December 2012 to April 2013, Pravec et al. (2014) showed Apophis has a non-principle axis rotation, and rebuilt its convex shape model, where the retrograde rotation period is $P_1 = 30.56$ h and the spin axis orientation is $(-75.0^\circ, 250.0^\circ)$. Pravec et al. (2014) also derived Apophis' average absolute visual magnitude to be $H_v = 19.09$ assuming the slope parameter to be $G = 0.24 \pm 0.11$.

Generally the thermal inertia of an asteroid can be evaluated by fitting thermal infrared observations with a thermophysical model to reproduce thermal emission curves. Following the shape model of Pravec et al. (2014), Müller et al. (2014) utilized the so-called thermophysical model (TPM) to analyze Apophis' Herschel-far-infrared observations, and derived its thermal inertia to be $250 - 800 \text{ Jm}^{-2}\text{s}^{-0.5}\text{K}^{-1}$ with a best solution about $600 \text{ Jm}^{-2}\text{s}^{-0.5}\text{K}^{-1}$, mean effective diameter 375_{-10}^{+14} m, and geometry albedo $0.30_{-0.06}^{+0.05}$. All

indicating that Apophis might also have a rubble-pile structure. However, recently Licandro et al. (2016) derived a relatively lower thermal inertia $50 - 500 \text{ Jm}^{-2}\text{s}^{-0.5}\text{K}^{-1}$ with a best solution of $\Gamma = 150 \text{ Jm}^{-2}\text{s}^{-0.5}\text{K}^{-1}$ and low surface roughness, indicating a surface material like that of Eros. Licandro et al. (2016) used the same TPM like Müller et al. (2014), but added three new mid-infrared data measured by CanariCam of Gran Telescopio CANARIAS. Both the work of Müller et al. (2014) and Licandro et al. (2016) assumed constant thermal emissivity to derive the surface thermophysical properties, but actually the thermal emissivity may be wavelength dependent from mid-infrared to far infrared (Müller & Lagerros, 1998), which should be taken into account when deriving the surface thermophysical properties.

In the present work, we utilize the independently developed thermophysical simulation codes (Yu, Ji & Wang, 2014; Yu & Ji, 2015) based on the frame work of Advanced Thermophysical Model (ATPM) (Rozitis & Green, 2011) to analyse the mid-infrared and far infrared data of Apophis observed by CanariCam and Herschel respectively. We show that if wavelength dependent emissivities are used, better solutions can be obtained, and the derived thermal inertia and effective diameter can be different from the results derived on the basis of constant emissivity. Moreover, we find that the surface of Apophis may be a high rough surface with low thermal inertia materials. The low thermal inertia of the small-size asteroid Apophis reveals that small-size asteroid may also have regolith on the surface, and further suggests that Apophis may be delivered from the Main Belt by Yarkovsky effect.

2 THERMOPHYSICAL MODELLING

2.1 Thermal infrared Observations

Until by now, the available thermal infrared measurements of Apophis are the far-IR data observed by the Herschel Space Observatory (Müller et al., 2014), and three mid-IR data measured by CanariCam of Gran Telescopio CANARIAS (Licandro et al., 2016). All these data are used in this work to be compared with the theoretical flux simulated from the so-called Advanced thermophysical Model so as to derive the possible scale of surface thermophysical properties. We tabulate data used in the fitting in Table 1.

2.2 Advanced thermophysical model

In ATPM Procedure (Rozitis & Green, 2011; Yu, Ji & Wang, 2014; Yu & Ji, 2015), we treat an asteroid to be a polyhedron composed of N triangle facets. For each facet, the roughness is modelled by a fractional coverage of hemispherical micro-craters, symbolized by f_r ($0 \leq f_r \leq 1$), whereas the remaining fraction, $1 - f_r$, represents a smooth flat surface. For such rough surface facet, the conservation of energy leads to an instant heat balance between sunlight, thermal emission, heat conduction, multiple-scattered sunlight and thermal-radiated fluxes from other facets. If each facet is small enough and far larger than the spatial scale of roughness, the heat conduction in that region can be approximatively described as one-dimensional (1D) heat conduction. Meanwhile, the temperature T_i of each facet varies with time as the asteroid rotates. In this process, T_i can be significantly affected by shading, multiple-scattered sunlight and thermal-radiated fluxes from other facets, which well explains the so-called thermal infrared beaming effect. When the entire asteroid comes into the final thermal equilibrium state, T_i will change periodically following the rotation of

Table 1 Observational data used in this work. (Müller et al., 2014; Licandro et al., 2016)

UT	Wavelength (μm)	Flux (mJy)	r_{helio} (AU)	Δ_{obs} (AU)	α ($^\circ$)	Observation Instrument
2013-01-06 00:10	70.0	36.3 \pm 1.1	1.03593	0.096247	+60.44	Herschel/PACS
2013-01-06 00:10	160.0	8.7 \pm 3.3	1.03593	0.096247	+60.44	Herschel/PACS
2013-01-06 00:44	100.0	22.8 \pm 1.7	1.03599	0.096234	+60.40	Herschel/PACS
2013-01-06 00:44	160.0	7.4 \pm 3.8	1.03599	0.096234	+60.40	Herschel/PACS
2013-01-06 01:15	70.0	37.5 \pm 1.3	1.03604	0.096221	+60.36	Herschel/PACS
2013-01-06 01:15	160.0	9.8 \pm 2.5	1.03604	0.096221	+60.36	Herschel/PACS
2013-01-06 01:47	100.0	25.0 \pm 1.5	1.03609	0.096208	+60.32	Herschel/PACS
2013-01-06 01:47	160.0	8.2 \pm 2.2	1.03609	0.096208	+60.32	Herschel/PACS
2013-03-14 06:40	70.0	12.6 \pm 2.7	1.093010	0.232276	-61.38	Herschel/PACS
2013-03-14 06:54	70.0	11.4 \pm 2.7	1.093003	0.232307	-61.38	Herschel/PACS
2013-03-14 07:07	70.0	10.4 \pm 2.7	1.092996	0.232338	-61.39	Herschel/PACS
2013-03-14 07:21	70.0	12.5 \pm 2.6	1.092989	0.232368	-61.39	Herschel/PACS
2013-03-14 07:35	70.0	13.3 \pm 2.7	1.092983	0.232397	-61.40	Herschel/PACS
2013-03-14 07:49	70.0	12.4 \pm 2.6	1.092976	0.232427	-61.40	Herschel/PACS
2013-01-29 22:04	12.5	240.0 \pm 20	1.079706	0.113407	-31.73	CanariCam/GTC
2013-01-29 23:09	17.65	310.0 \pm 70	1.079761	0.113478	-31.74	CanariCam/GTC
2013-01-29 23:52	8.70	140.0 \pm 10	1.079816	0.113549	-31.75	CanariCam/GTC

For a given observation epoch, ATPM can reproduce a theoretical profile to each observation flux as:

$$F_{\text{model}}(\lambda) = \sum_{i=1}^N \epsilon(\lambda) S(i) f(i) B(\lambda, T_i), \quad (1)$$

where $\epsilon(\lambda)$ is the monochromatic emissivity at wavelength λ , $S(i)$ is the area of facet i , $f(i)$ is the view factor of facet i to the telescope

$$f(i) = v_i \frac{\mathbf{n}_i \cdot \mathbf{n}_{\text{obs}}}{\pi \Delta^2}, \quad (2)$$

$v_i = 1$ indicates facet i is visible (otherwise $v_i = 0$), and $B(\lambda, T_i)$ is the Planck function:

$$B(\lambda, T_i) = \frac{2\pi h c^2}{\lambda^5} \frac{1}{\exp\left(\frac{hc}{\lambda k T_i}\right) - 1}. \quad (3)$$

Thus the calculated F_{model} can be compared with the thermal infrared fluxes summarized in Table 1 in the fitting process.

2.3 Fitting Procedure

In order to derive the thermophysical properties of Apophis via the ATPM procedure, several physical parameters are needed, including the 3D shape model, effective diameter D_{eff} , and the so-called thermal parameter

$$\Phi = \frac{\Gamma \sqrt{\omega}}{\quad} \quad (4)$$

where ω is the rotation frequency, Γ is the thermal inertia, ε is the averaged thermal emissivity over the entire emission spectrum, and

$$T_{\text{eff}} = \left[\frac{(1 - A_B)F_{\odot}}{\varepsilon\sigma d_{\odot}^2} \right]^{1/4},$$

is the effective temperature. The rotation frequency ω can be easily determined from light curves, while thermal inertia Γ is the parameter of interest which would be treated as free parameter in the fitting procedure.

We can employ the light-curve inversion 3D shape model of Apophis rebuilt by Pravec et al. (2014) (Figure 1) in our fitting procedure. According to Fowler & Chillemi (1992), an asteroid's effective diameter

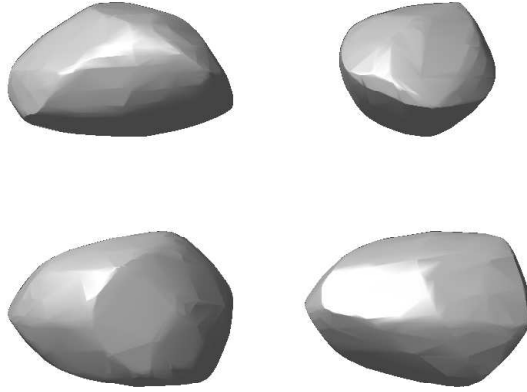


Fig. 1 The 3D shape model of Apophis utilized in this work is the light-curve inversion shape rebuilt by Pravec et al. (2014).

D_{eff} , defined by the diameter of a sphere with a identical volume to that of the shape model, can be related to its geometric albedo p_v and absolute visual magnitude H_v via:

$$D_{\text{eff}} = \frac{1329 \times 10^{-H_v/5}}{\sqrt{p_v}} \text{ (km)}. \quad (5)$$

In addition, the geometric albedo p_v is related to the effective Bond albedo $A_{\text{eff,B}}$ by

$$A_{\text{eff,B}} = p_v q_{\text{ph}}, \quad (6)$$

where q_{ph} is the phase integral that can be approximated by (Bowell et al., 1989)

$$q_{\text{ph}} = 0.290 + 0.684G, \quad (7)$$

in which G is the slope parameter in the H, G magnitude system of Bowell et al. (1989). We use $H_v = 19.09 \pm 0.19$, $G = 0.24 \pm 0.11$, the results of Pravec et al. (2014) in the fitting procedure.

On the other hand, the asteroid's effective Bond albedo is the averaged result of both the albedo of smooth and rough surface, which can be expressed as the following relationship:

$$A_{\text{eff,B}} = (1 - \epsilon)A_{\text{smooth}} + \epsilon A_B \quad (8)$$

where A_B is the Bond albedo of smooth lambertian surface, which should be related to the composition of surface materials. Thus a input roughness fraction f_r and geometric albedo p_v can lead to a unique Bond albedo A_B and effective diameter D_{eff} to be used to fit the observations.

Then we have three free parameters — thermal inertia, roughness fraction, and geometric albedo (or effective diameter) that would be extensively investigated in the fitting process. Other parameters are listed in Table 2.

Table 2 Assumed physical parameters used in ATPM.

Property	Value	References
Number of vertices	1014	(Pravec et al., 2014)
Number of facets	2024	(Pravec et al., 2014)
Shape (a:b:c)	1.1135:1.0534:1	(Pravec et al., 2014)
Angular momentum vector	(-75.0° , 250.0°)	(Pravec et al., 2014)
Spin period	30.56 h	(Pravec et al., 2014)
Absolute magnitude	19.09 ± 0.19	(Pravec et al., 2014)
Slope parameter	0.24 ± 0.11	(Pravec et al., 2014)
Thermal emissivity	0.9	assumption

It should be also noticed here that the utilized observation data are observed at various wavelength from mid-infrared to far-infrared, thus it may be no longer suitable to assume an average constant emissivity for all wavelength when calculating flux by Equation (1), because the spectral emissivity may differ with wavelength from mid-infrared to far-infrared (Müller & Lagerros, 1998). Therefore the spectral emissivity ϵ remains to be a free parameter as well.

For the input free parameters, we use an initial geometric albedo $p_v = 0.3$, but scan thermal inertia Γ in the range $0 \sim 500 \text{ Jm}^{-2}\text{s}^{-0.5}\text{K}^{-1}$, and roughness fraction f_r in the range $0.0 \sim 1.0$. For the spectral emissivity ϵ , we firstly assume it to be constant 0.9 (CE for short), then vary it to see if we can get better solutions. For each pair of (Γ, f_r) , we could find a new p_v (or D_{eff}) that gives a minimum reduced χ^2 defined as

$$\chi_r^2 = \frac{1}{n-3} \sum_{i=1}^n \left[\frac{F_{\text{model}}(\lambda_i, \Gamma, f_r, p_v) - F_{\text{obs}}(\lambda_i)}{\sigma_{\lambda_i}} \right]^2, \quad (9)$$

which is used to assess the fitting degree of our model with respect to the observations. Herein the predicted model flux F_{model} is a rotationally averaged profile assuming the rotation along the angular momentum vector, for the rotation phases of Apophis at the time of observation are uncertain due to its non-principal axis rotation. Through the rotationally averaged procedure, the influence arising from the tumbling rotation would somewhat decrease, but the thermal properties can be well revealed from the seasonal effect, because we have observations at different epochs.

3 ANALYSIS AND RESULTS

As mentioned above, we firstly assume the spectral emissivity to be constant 0.9 for each observed wave-

Table 3 ATPM fitting results to the observations with constant spectral emissivity = 0.9 for each wavelength.

Roughness		Thermal inertia Γ ($\text{Jm}^{-2}\text{s}^{-0.5}\text{K}^{-1}$)												
fraction	0	50		100		150		200		250		300		
f_R	p_v	χ_r^2	p_v	χ_r^2	p_v	χ_r^2	p_v	χ_r^2	p_v	χ_r^2	p_v	χ_r^2	p_v	χ_r^2
0.00	0.316	4.64	0.342	5.49	0.346	5.94	0.347	6.33	0.347	6.70	0.347	7.08	0.347	7.42
0.05	0.313	4.46	0.335	5.28	0.338	5.73	0.339	6.12	0.339	6.49	0.339	6.88	0.339	7.23
0.10	0.312	4.29	0.335	5.08	0.337	5.53	0.338	5.92	0.338	6.29	0.338	6.68	0.338	7.04
0.15	0.312	4.12	0.334	4.89	0.337	5.33	0.337	5.72	0.337	6.10	0.337	6.49	0.337	6.86
0.20	0.311	3.97	0.333	4.70	0.336	5.13	0.336	5.52	0.336	5.90	0.336	6.31	0.336	6.67
0.25	0.310	3.84	0.333	4.53	0.335	4.95	0.336	5.34	0.335	5.72	0.335	6.12	0.335	6.49
0.30	0.310	3.71	0.332	4.36	0.334	4.77	0.335	5.15	0.334	5.53	0.334	5.94	0.334	6.32
0.35	0.309	3.60	0.331	4.20	0.333	4.59	0.334	4.98	0.333	5.36	0.333	5.77	0.333	6.15
0.40	0.308	3.49	0.330	4.04	0.332	4.43	0.333	4.80	0.332	5.18	0.332	5.60	0.332	5.98
0.45	0.307	3.40	0.330	3.89	0.331	4.27	0.332	4.64	0.331	5.01	0.331	5.43	0.331	5.82
0.50	0.306	3.32	0.329	3.75	0.330	4.11	0.330	4.48	0.330	4.85	0.330	5.27	0.329	5.65
0.55	0.305	3.25	0.328	3.62	0.329	3.96	0.329	4.32	0.329	4.69	0.328	5.11	0.328	5.50
0.60	0.304	3.19	0.326	3.49	0.328	3.82	0.328	4.17	0.327	4.54	0.327	4.95	0.326	5.34
0.65	0.303	3.14	0.325	3.37	0.327	3.68	0.326	4.02	0.326	4.39	0.326	4.80	0.325	5.19
0.70	0.302	3.10	0.324	3.26	0.325	3.55	0.325	3.88	0.324	4.24	0.324	4.65	0.323	5.04
0.75	0.300	3.07	0.323	3.15	0.324	3.43	0.323	3.75	0.323	4.10	0.322	4.51	0.322	4.90
0.80	0.299	3.05	0.321	3.05	0.322	3.31	0.322	3.61	0.321	3.96	0.321	4.37	0.320	4.76
0.85	0.297	3.05	0.319	2.96	0.320	3.19	0.320	3.49	0.319	3.83	0.319	4.23	0.318	4.62
0.90	0.296	3.05	0.318	2.87	0.319	3.08	0.318	3.37	0.317	3.70	0.317	4.10	0.316	4.48
0.95	0.294	3.06	0.316	2.79	0.317	2.98	0.316	3.25	0.315	3.57	0.315	3.97	0.314	4.35
1.00	0.290	3.08	0.318	2.71	0.319	2.88	0.318	3.14	0.317	3.45	0.316	3.84	0.315	4.22

From Table 3, we can see that low thermal inertia and high roughness fraction tend to fit better to the observations; the best-fit solution, corresponding to the lowest reduced χ_r^2 arises at about $p_v = 0.318$ $\Gamma = 50 \text{ Jm}^{-2}\text{s}^{-0.5}\text{K}^{-1}$ and $f_r = 1.0$. With this result, we plot the ratio of 'observation/model' to examine how these theoretical model results match the observations at various wavelengths (Figure 2).

In Figure 2, we can see that the ratios at each wavelength are not randomly distributed around 1.0, but reveal a wavelength dependent feature like the red fitting curve, where the maximum ratio may arise around $20 \mu\text{m}$. This feature implies that the spectral emissivity used in Equation (1) should not be a constant $\epsilon(\lambda) \equiv 0.9$, but should be wavelength dependent, where the maximum emissivity may arise around $20 \mu\text{m}$. Thus we should introduce a wavelength dependent spectral emissivity $\epsilon(\lambda)$ to do the fitting process again.

Müller & Lagerros (1998) reported the wavelength dependent spectral emissivity of asteroid Ceres and Vesta. As the spectral feature of Vesta may be much closer to Apophis than Ceres, so we imagine that the Apophis' emissivity changes with wavelength in a similar way like that of asteroid Vesta (Müller & Lagerros, 1998) as showed in Table 4. With these wavelength dependent emissivity, we did get

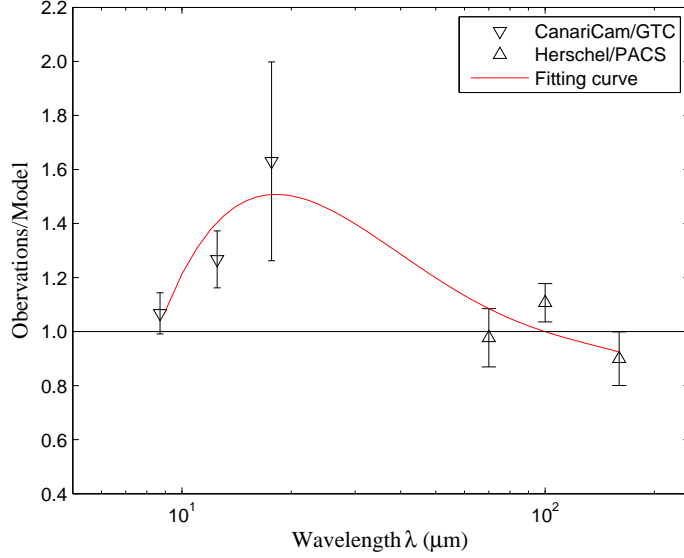


Fig. 2 The observation/model ratios as a function of wavelength for $\Gamma = 50 \text{ Jm}^{-2}\text{s}^{-0.5}\text{K}^{-1}$, $f_r = 1.0$, $p_v = 0.318$, and $D_{\text{eff}} = 382 \text{ m}$ when using $\epsilon(\lambda) \equiv 0.9$. The ratios with their errors at each wavelength are all error-weighted average results. The red fitting curve is obtained from a 4th degree polynomial fitting for $x = \log 10(\lambda)$, $y = F_{\text{obs}}/F_{\text{model}}$.

Table 4 Assumed Emissivity for different wavelength.

Wavelength	Emissivity
8.7, 12.5 μm	0.90
17.65 μm	0.96
70, 100 μm	0.80
160 μm	0.75

Table 5 summarises the reduced χ_r^2 obtained from each input pair of thermal inertia and roughness fraction when using the emissivity given in Table 4. We can see that, in this case, high roughness fraction tends to fit better as well. But the best-fit thermal inertia and geometric albedo shift to $\Gamma = 100 \text{ Jm}^{-2}\text{s}^{-0.5}\text{K}^{-1}$ and $p_v = 0.286$ respectively. We compared the reduced χ_r^2 obtained from the two case CE and WDE in Figure 3, where the black curves represent the reduced χ^2 obtained from constant emissivity input while the red curves stand for wavelength dependent emissivity. We can see that the obtained minimum reduced χ_r^2 can be significantly lower when the WDE are used to fit observations, indicating that the spectral emissivity of Apophis should be wavelength dependent.

Table 5 ATPM fitting results to the observations with wavelength dependent emissivity.

Roughness			Thermal inertia Γ ($\text{Jm}^{-2}\text{s}^{-0.5}\text{K}^{-1}$)																			
fraction	0		50		100		150		200		250		300		350		400		450		500	
f_R	p_v	χ_R^2	p_v	χ_R^2	p_v	χ_R^2	p_v	χ_R^2	p_v	χ_R^2	p_v	χ_R^2	p_v	χ_R^2	p_v	χ_R^2	p_v	χ_R^2	p_v	χ_R^2	p_v	χ_R^2
0.00	0.283	3.64	0.305	4.18	0.308	4.55	0.309	4.89	0.309	5.22	0.309	5.57	0.308	5.89	0.308	6.21	0.307	6.52	0.306	6.80	0.306	7.09
0.05	0.284	3.52	0.304	4.01	0.306	4.37	0.307	4.70	0.307	5.03	0.307	5.38	0.306	5.70	0.306	6.03	0.306	6.34	0.305	6.63	0.305	6.93
0.10	0.284	3.40	0.304	3.84	0.306	4.19	0.307	4.52	0.306	4.84	0.306	5.20	0.306	5.52	0.305	5.85	0.305	6.17	0.304	6.46	0.304	6.76
0.15	0.284	3.31	0.304	3.68	0.306	4.02	0.306	4.34	0.306	4.66	0.306	5.02	0.305	5.35	0.305	5.68	0.304	6.00	0.304	6.30	0.303	6.60
0.20	0.283	3.22	0.303	3.53	0.305	3.85	0.305	4.17	0.305	4.49	0.305	4.84	0.305	5.18	0.304	5.51	0.304	5.84	0.303	6.14	0.303	6.45
0.25	0.283	3.15	0.303	3.40	0.305	3.70	0.305	4.00	0.305	4.32	0.304	4.68	0.304	5.01	0.303	5.35	0.303	5.68	0.302	5.98	0.302	6.30
0.30	0.282	3.10	0.302	3.27	0.304	3.55	0.304	3.84	0.304	4.16	0.304	4.51	0.303	4.85	0.303	5.19	0.302	5.52	0.301	5.82	0.301	6.14
0.35	0.282	3.06	0.302	3.14	0.303	3.41	0.304	3.69	0.303	4.00	0.303	4.35	0.302	4.69	0.302	5.03	0.301	5.37	0.301	5.67	0.300	6.00
0.40	0.281	3.03	0.301	3.03	0.303	3.27	0.303	3.55	0.302	3.85	0.302	4.20	0.301	4.54	0.301	4.88	0.300	5.22	0.300	5.52	0.299	5.85
0.45	0.281	3.01	0.301	2.93	0.302	3.15	0.302	3.41	0.301	3.71	0.301	4.05	0.300	4.39	0.300	4.73	0.299	5.07	0.299	5.38	0.298	5.71
0.50	0.280	3.01	0.300	2.83	0.301	3.03	0.301	3.28	0.300	3.57	0.300	3.91	0.299	4.24	0.299	4.58	0.298	4.92	0.298	5.23	0.297	5.57
0.55	0.279	3.02	0.299	2.74	0.300	2.92	0.300	3.15	0.299	3.43	0.299	3.77	0.298	4.10	0.298	4.44	0.297	4.78	0.296	5.09	0.296	5.43
0.60	0.279	3.04	0.298	2.66	0.299	2.81	0.299	3.03	0.298	3.30	0.298	3.63	0.297	3.96	0.297	4.30	0.296	4.64	0.295	4.95	0.295	5.29
0.65	0.278	3.07	0.298	2.59	0.298	2.71	0.298	2.92	0.297	3.18	0.297	3.50	0.296	3.82	0.295	4.16	0.295	4.51	0.294	4.82	0.294	5.16
0.70	0.277	3.12	0.297	2.53	0.297	2.62	0.297	2.81	0.296	3.06	0.296	3.38	0.295	3.69	0.294	4.03	0.294	4.37	0.293	4.69	0.292	5.03
0.75	0.276	3.17	0.296	2.47	0.296	2.54	0.296	2.71	0.295	2.94	0.294	3.25	0.293	3.57	0.293	3.90	0.292	4.24	0.291	4.56	0.291	4.90
0.80	0.275	3.24	0.294	2.42	0.295	2.46	0.294	2.61	0.293	2.83	0.293	3.14	0.292	3.44	0.291	3.78	0.291	4.12	0.290	4.43	0.290	4.78
0.85	0.274	3.32	0.293	2.38	0.294	2.38	0.293	2.52	0.292	2.73	0.291	3.02	0.290	3.33	0.290	3.65	0.289	3.99	0.288	4.31	0.288	4.65
0.90	0.273	3.42	0.292	2.34	0.292	2.32	0.291	2.43	0.290	2.63	0.290	2.91	0.289	3.21	0.288	3.53	0.288	3.87	0.287	4.18	0.286	4.53
0.95	0.272	3.52	0.291	2.32	0.291	2.26	0.290	2.35	0.289	2.53	0.288	2.81	0.287	3.10	0.286	3.42	0.286	3.76	0.285	4.07	0.285	4.41
1.00	0.263	3.63	0.286	2.30	0.286	2.21	0.285	2.28	0.284	2.44	0.283	2.71	0.282	2.99	0.281	3.31	0.280	3.64	0.279	3.95	0.278	4.30

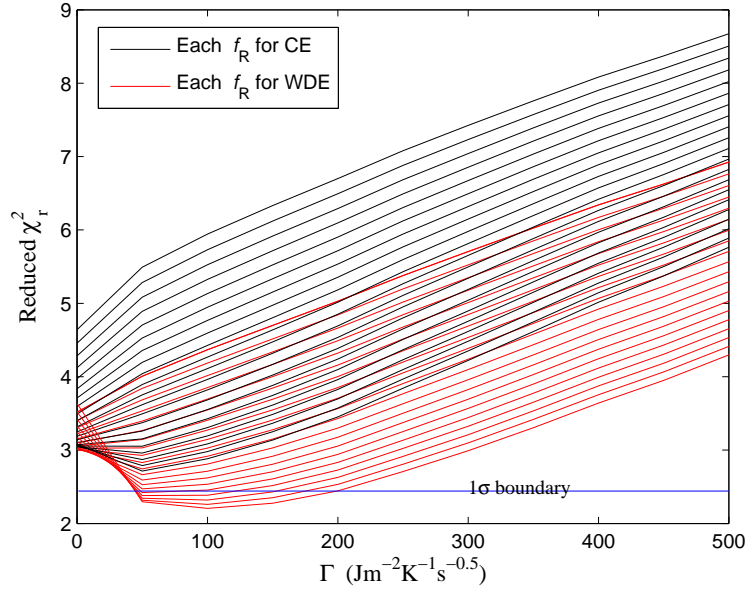


Fig. 3 $\Gamma \sim \chi_r^2$ curves for both the CE (constant emissivity) and WDE (wavelength dependent emissivity) cases considering $f_r = 0.0 \sim 1.0$.

Since we can not obtain best solutions by assuming constant emissivity, then we have no reason to fit the observations with ATPM by using constant emissivity. Therefore we adopt the wavelength dependent emissivity similar to that of asteroid Vesta to further derive the surface thermal inertia, roughness fraction and geometric albedo here.

Figure 4 shows the contour of $\chi_r^2(f_r, \Gamma)$ according to Table 5, where the color variation from blue to red means the increase of the reduced χ_r^2 . The deep blue curve labelled by 1σ corresponds to $\Delta\chi_r^2 = 0.252$ from the minimum χ_r^2 , constraining the scale of the free parameters with possibility about 68.3%, whereas the blue curve labelled by 3σ refers to $\Delta\chi_r^2 = 1.014$, giving the scale of free parameters with possibility about 99.73% (Press et al., 2007).

Figure 5 shows the $p_v \sim \chi_r^2$ obtained in consideration of the above derived Γ and f_r as well as the absolute visual magnitude $H_v = 19.09 \pm 0.19$, where the 1σ and 3σ limits are the same as above. The scale of absolute visual magnitude H_v does not affect the distribution of reduced χ_r^2 derived from each pair of thermal inertia and roughness fraction, but has significant influence on the corresponding geometric albedo and effective diameter. Thus we do not treat H_v as free parameters, but consider its influence by only using the upper limit, mid-value and lower limit of H_v , each was adopted to be a constant in the fitting process. And the final results of geometric albedo and effective diameter are constrained by considering three cases of H_v together, leading to the 1σ and 3σ scales non-Gaussian.

Using the assumed wavelength dependent emissivity in Table 4, we can derive thermal inertia Γ , roughness fraction f_r , geometric albedo p_v and effective diameter D_{eff} , where are considered be free parameters

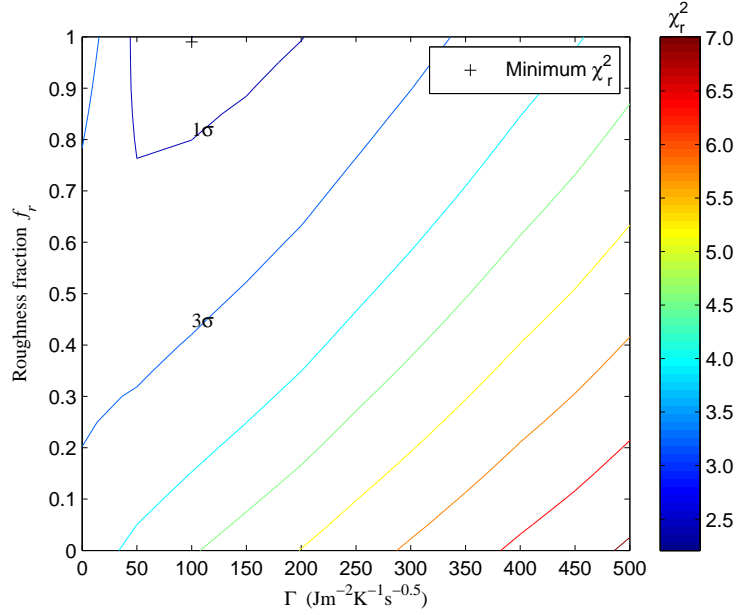


Fig. 4 $\chi_r^2(f_r, \Gamma)$ contour according to Table 5. The color (from blue to red) means the increase of profile of χ_r^2 . 1σ corresponds to $\Delta\chi_r^2 = 0.252$, while 3σ corresponds to $\Delta\chi_r^2 = 1.014$ (Press et al., 2007).

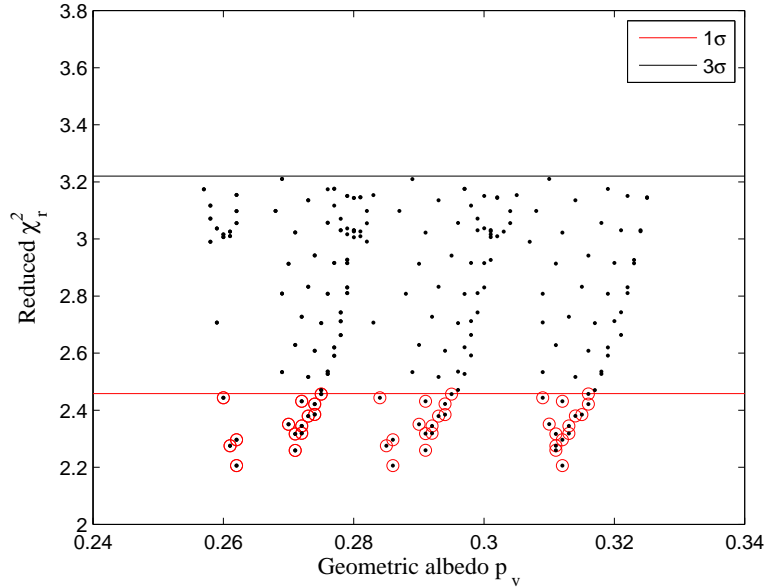


Fig. 5 $p_v \sim \chi_{\text{reduced}}^2$ profiles fit to the observations in consideration of the derived 1σ and 3σ range of f_r and Γ and the absolute visual magnitude $H_v = 19.09 \pm 0.19$.

4 DISCUSSION AND CONCLUSION

In this work, the mid-infrared and far-infrared data of Apophis observed by CanariCam on Gran Telescopio CANARIAS and PACS of Herschel are analysed by the Advanced thermophysical model (ATPM), where

Table 6 The derived parameters for Apophis.

Properties	1 σ scale	3 σ scale
Thermal inertia Γ ($\text{Jm}^{-2}\text{s}^{-0.5}\text{K}^{-1}$)	100_{-52}^{+100}	100_{-100}^{+240}
Roughness fraction f_r	0.78~1.0	0.2~1.0
Geometric albedo p_v	$0.286_{-0.026}^{+0.03}$	$0.286_{-0.029}^{+0.039}$
Effective diameter D_{eff} (m)	378_{-25}^{+19}	378_{-29}^{+27}

are investigated. We found that the thermal emissivity of Apophis should be wavelength dependent, and using a similar emissivity like that of Vesta could obtain better degree of fitting. As a result, we derive the thermal inertia, roughness fraction, geometric albedo and effective diameter of Apophis in a possible 1 σ scale of $\Gamma = 100_{-52}^{+100} \text{ Jm}^{-2}\text{s}^{-0.5}\text{K}^{-1}$, $f_r = 0.78 \sim 1.0$, $p_v = 0.286_{-0.026}^{+0.030}$, $D_{\text{eff}} = 378_{-25}^{+19}$ m, and 3 σ scale of $\Gamma = 100_{-100}^{+240} \text{ Jm}^{-2}\text{s}^{-0.5}\text{K}^{-1}$, $f_r = 0.2 \sim 1.0$, $p_v = 0.286_{-0.029}^{+0.039}$, $D_{\text{eff}} = 378_{-29}^{+27}$ m. The derived thermal inertia supports the result of Licandro et al. (2016) despite a little lower. The best fit high roughness is different from the result of Licandro et al. (2016), but is inconsistent with with the work of Müller et al. (2014) where the best fit solution also supports a high roughness.

To verify the the reliability of our fitting procedure and derived outcomes, we employ the ratio of 'observation/model' (Müller et al., 2005, 2011, 2012) to examine how these theoretical model results match the observations at various wavelengths (see Figure 6). In Figure 6, the observation/Model ratios are shown at each observational wavelength for $f_r = 1.0$, $\Gamma = 100 \text{ Jm}^{-2}\text{s}^{-0.5}\text{K}^{-1}$, $p_v = 0.286$ and $D_{\text{eff}} = 378$ m. The ratios are distributed more nearly around 1.0 compared to Figure 2, despite the ratios at $17.65 \mu\text{m}$ move relatively larger than unity which again support the idea that Apophis' spectral emissivity should be wavelength dependent. However, we can not know how exactly the spectral emissivity varies with wavelength at present, for the available spectral data is not enough. If, in the future, more spectral data observed from mid-infrared to far-infrared are obtained, we may find out how the emissivity of Apophis depends on wavelength.

Given the low gravitational acceleration on the surface of asteroids, it was generally thought that regolith formation would not be possible, especially on small-size asteroids. The statistical results of thermal inertia versus the size of asteroids in the work of Delbo et al. (2007) suggest that small-size asteroid should have high thermal inertia, indicating rocky surface, also support the above idea. But regolith on the small-size asteroid Itokawa was detected by the Hayabusa spacecraft, which suggests that regolith formation on asteroids, even small-size asteroids is also possible. The low thermal inertia result of Apophis in this work somewhat adds a good support to the idea that regolith formation may be not dominated by the size of asteroid. If a small asteroid has experienced enough long process of space weathering, the presence of regolith should be also reasonable. On the other hand, the size of Apophis is similar to asteroid Itokawa indicative of similar dynamical lifetime in principle. But the derived thermal inertia of Apophis is much lower than the observed thermal inertia of Itokawa (Müller et al., 2005), indicating Apophis may actually either exit

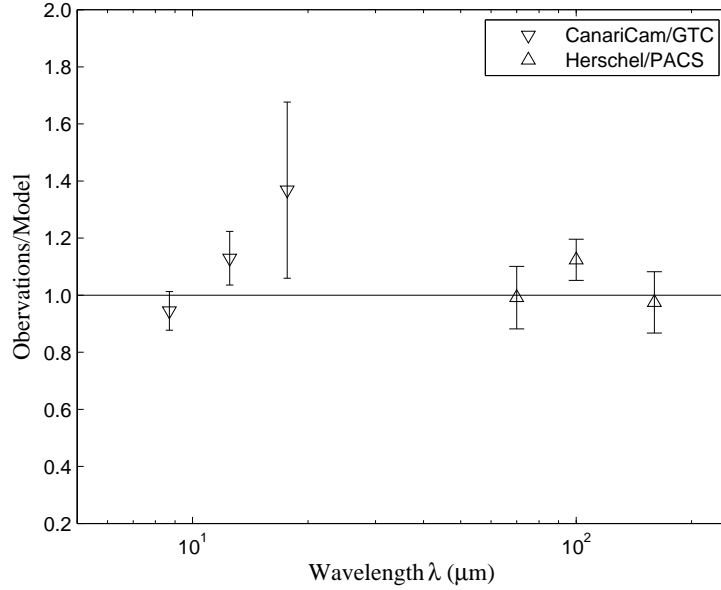


Fig. 6 The observation/model ratios as a function of wavelength for $\Gamma = 100 \text{ Jm}^{-2}\text{s}^{-0.5}\text{K}^{-1}$, $f_r = 1.0$, $p_v = 0.286$ and $D_{\text{eff}} = 378 \text{ m}$ in consideration of wavelength dependent emissivity. The ratios with their errors at each wavelength are all error-weighted average results.

retained over the surface. We notice that Apophis has much slower rotation $P_{\text{rot}} \approx 30.56 \text{ hr}$ than Itokawa ($P_{\text{rot}} \approx 12.13 \text{ hr}$), which may account for Apophis' lower thermal inertia, for the produced dust should be more easy to accumulate on a slow-rotating asteroid.

Generally rough surface would generate stronger Yarkovsky orbit drift than smooth surface (Rozitis & Green, 2012). Thus the Yarkovsky effect induced decreasing rate of Apophis' semimajor axis should be even larger than the predicted value of Vokrouhlický et al. (2015), because our results show Apophis tends to have a high-roughness surface, which should be taken into account to predict its orbit movement. Besides it is possible that Apophis may be one Vesta's fragment delivered from the Main Belt by Yarkovsky effect, in consideration of its long existence time suggested by low thermal inertia, and similar surface properties to Vesta implied by albedo and thermal emissivity.

In conclusion, when we attempt to investigate surface thermophysical properties of a target asteroid by utilizing thermal infrared radiometric method to fit observed data from mid-infrared to far-infrared, constant emissivity may be not always the best choice. For asteroid Apophis, the combined data of mid-infrared of CanariCam and far-infrared of Herschel reveals possible wavelength dependent thermal emissivity from $8.70 \mu\text{m}$ to $160 \mu\text{m}$, where the maximum emissivity may arise around $20 \mu\text{m}$ like that of Vesta, because this kind of emissivity can achieve better degree of fitting through the use of Advanced thermophysical model. Besides the derived results of low thermal inertia $\Gamma = 100_{-100}^{+240} \text{ Jm}^{-2}\text{s}^{-0.5}\text{K}^{-1}$ and high roughness fraction $f_r = 0.2 \sim 1.0$ indicate that Apophis may have experienced a long process of space weathering, but less regolith migration process, making the produced dust able to stay over its surface. These new deductions would be important for predicting Apophis' orbital movement and potential Earth impact probability so as

Acknowledgements We thank the anonymous referee for good comments and suggestions that helped to improve the manuscript. This work is financially supported by National Natural Science Foundation of China (Grants No. 11473073, 11403105, 11661161013), the Science and Technology Development Fund of Macau (Grants No. 039/2013/A2, 017/2014/A1), the innovative and interdisciplinary program by CAS (Grant No. KJZD-EW-Z001), the Natural Science Foundation of Jiangsu Province (Grant No. BK20141509), and the Foundation of Minor Planets of Purple Mountain Observatory.

References

- Abe, S., Mukai, T., Hirata, N., et al. 2006, *Science*, 312, 1344
- Binzel, R. P., Rivkin, A. S., Thomas, C. A., et al. 2009, *Icarus*, 200, 480
- Britt, D. T., Yeomans, D., Housen, K., & Consolmagno, G. 2002, *Asteroid Density, Porosity, and Structure*. In *Asteroids III*, eds. W. F. Bottke Jr., A. Cellino, P. Paolicchi, & R. P. Binzel (Tucson: University of Arizona Press), 485
- Britt, D. T., & Consolmagno, G. 2003, *Meteoritics*, 38, 1161
- Bottke, W.F., Vokrouhlický, D., Rubincam, D.P., Nesvorný, D., 2006. The Yarkovsky and YORP effects: Implications for asteroid dynamics. *Annu. Rev. Earth Planet. Sci.* 34, 157-191
- Bottke, W.F., et al. 2015, *Icarus*, 247, 191-217
- Bowell, E., Hapke, B., Domingue, D., et al., 1989, Application of photometric models to asteroids. In *Asteroids II*, pp. 524-556
- Chamberlain, M.A., Lovell, A.J., Sykes, M.V., 2007, *Icarus*, 192, 448-459
- Chesley, S.R., 2005. Potential impact detection for near-Earth asteroids: The case of 99942 Apophis (2004 MN 4). In: *IAU Symposium No. 229*, pp. 215-228.
- Conel, James E., 1969, Experimental results and a cloudy atmospheric model of spectral emission from condensed particulate mediums, *JGR*, 74, 1614-1634
- Delbo, M., Oro, A., Harris, A.W., Mottola, S., & Muller, M., 2007, *Icarus*, 190, 236-249
- Farnocchia, D. et al., 2013. Yarkovsky-driven impact risk analysis for Asteroid (99942) Apophis. *Icarus* 224, 192-200
- Fujiwara, A., Kawaguchi, J., Yeomans, D.K., et al, 2006, *Science*, 312, 1330-1334
- Fowler, J.W., & Chillemi, J.R., 1992, IRAS asteroids data processing. In *The IRAS Minor Planet Survey*, pp. 17-43
- Gilmore, A.C. et al., 2004. 2004 MN4. *Minor Planet Electronic Circulars Y*, 25
- Giorgini, J.D., Benner, L.A.M., Ostro, S.J., Nolan, M.C., Busch, M.W., 2008. Predicting the Earth encounters of (99942)Apophis. *Icarus* 193, 1-19
- Lagerros, J.S.V., 1996, *A&A*, 310, 1011-1020
- Lagerros, J.S.V., 1996, *A&A*, 315, 625-632
- Licandro, J., Müller, T.G., Alvarez, C. et al, 2016, *A&A*, 585, A10
- Müller, T.G., & Lagerros, J.S.V., 1998, *A&A*, 338, 340-352
- Müller, T.G., 2002, *Meteor. Planet. Sci.*, 37, 1919

- Müller, T.G., Durech, J., Hasegawa, S., et al., 2011, *A&A*, 525, A145
- Müller, T.G., O'Rourke, L., Barucci, A.M., et al., 2012, *A&A*, 548, A36
- Müller, T.G., Kiss, C., Scheirich, P., et al., 2014, *A&A*, 566, A22
- Opeil, C.P., Consolmagno, G.J., Safarik, D.J., Britt, D.T., 2012, *Meteorit. Planet. Sci.* 47, 319-329
- Ostro, S.J., Hudson, R.S., Rosema, K.D., et al., 1999, *Icarus* 137, 122-139
- Pravec, P., Scheirich, P., Durech, J., et al., 2014, *Icarus*, 233, 48-60
- Press W.H., et al., *Numerical Recipes*, 3th Edition, 2007, Cambridge University Press, New York, p. 815
- Rozitis, B., & Green, S.F., 2011, *MNRAS*, 415, 2042
- Rozitis, B., & Green, S.F., 2012, *MNRAS*, 423, 367
- Saito J., Miyamoto H., Nakamura R. Detailed Images of Asteroid 25143 Itokawa from Hayabusa. *Science*, 2006, 312: 1341
- Thuillot, W., Bancelin, D, Ivantsov, A., et al., 2015, *A&A*, 583, A59
- Vokrouhlický, D., Farnocchia, D., Čapek, D., et al., 2015, *Icarus*, 252, 277-283
- Wang, N., Peng, Q.Y., Zhang, X.L., et al., 2015, *MNRAS*, 454, 3805-3809
- Yu, L.L., Ji, J.H., & Wang, S., 2014, *MNRAS*, 439, 3357-3370
- Yu, L.L., & Ji, J.H., 2015, *MNRAS*, 452, 368-375